Sensors and Actuators A 244 (2016) 44–49

Contents lists available at ScienceDirect

Sensors and Actuators A: Physical

journal homepage: www.elsevier.com/locate/sna

A coaxial probe with a vertically split outer sensor for charge and dimensional measurement of a passing object

Janne Peltonen[a,b,*], Matti Murtomaa[a], Aleksi Saikkonen[a], Jarno Salonen[a]

[a] Department of Physics and Astronomy, University of Turku, 20014 Turku, Finland
[b] University of Turku Graduate School, University of Turku, 20014 Turku, Finland

ARTICLE INFO

Article history:
Received 7 December 2015
Received in revised form 24 March 2016
Accepted 5 April 2016
Available online 6 April 2016

Keywords:
Charge measurement
Size measurement
Distance measurement
Electrostatic charging
Instrumentation
Simulations

ABSTRACT

A coaxial induction probe with a vertically split outer sensor for simultaneously measuring the charge, distance, and size of a passing object is presented. When a charged sphere passed the probe, current signals of different shape induced to all the sensors. The signals were integrated, and Gaussian curves were fitted. The amplitudes and widths of the fitted curves were used to calibrate the set-up. The experimental calibration was done by using frictionally charged spheres of different sizes. Spheres with unknown size, distance, and charge were measured using the calibrated sensor. However, the speed of the object needed to be known. The results from computer simulations, calibrations, and use in measurements are presented.

1. Introduction

In industry, triboelectric charging causes many undesirable effects. These effects include adhesion on the surfaces [1,2], electrostatic discharges (ESD) [3,4], and dust explosions [5,6]. On the other hand, many useful applications, such as electrostatic powder coating, paint spraying or electrostatic precipitation, are based on controlled movement of charged particles [7]. Since many parameters, such as material properties and environmental conditions, affect the charging processes, a good method for measuring the charge is necessary. Reliable data would also enable the development of the theory behind charging. One of the most widely used method for measuring the electric charge of solid particles is the Faraday cup [8–10] which is also suitable for measuring the charge of electron and ion beams [11–13]. In cases where only the net charge is of interest, Faraday cups are valuable and reliable instruments. However in some applications, for instance when charge density is of interest, the size of the object is also important to know. Also, for moving particles, the particle position and speed can be essential parameters.

A coaxial induction probe for measuring the charge, size, and distance of a passing object was previously presented, with promising results [14,15]. The probe was not only used to measure these properties for frictionally charged spheres, but also to measure the charge-to-mass ratio of fluidized powders in a fluidized bed system. This was possible since the signals arising from a charged object were similar to the signals caused by a bubble in a charged powder. According to recent computer simulations, the probe could be further improved by modifying geometry of the coaxial sensor. In this work, we present both simulational and experimental results obtained by using the new probe geometry to measure passing charged spheres. Machida et al. [16] developed a tomography system based on induced currents caused by a charged particle. Similarly to this study, also they had a probe attached to a metal pipe wall. However, the location of the passing charge was measured using several sensors in different positions. In the present study, this method was not used in order to ensure that the measured signals arose from the same object. This is relevant when using a larger pipe with several charged objects. In this case it is not essential to detect all of them but only a portion.

2. Methods

2.1. Simulations

The previous probe consisted of a circular inner sensor (radius 1 mm) surrounded by a ring-shaped outer sensor (outer radius 3 mm, thickness 1 mm), separated from each other with an insulator. The probe was placed at the inner surface of a steel pipe filled

* Corresponding author at: Department of Physics and Astronomy, University of Turku, 20014 Turku, Finland.
E-mail address: janne.m.peltonen@utu.fi (J. Peltonen).

http://dx.doi.org/10.1016/j.sna.2016.04.014
0924-4247/

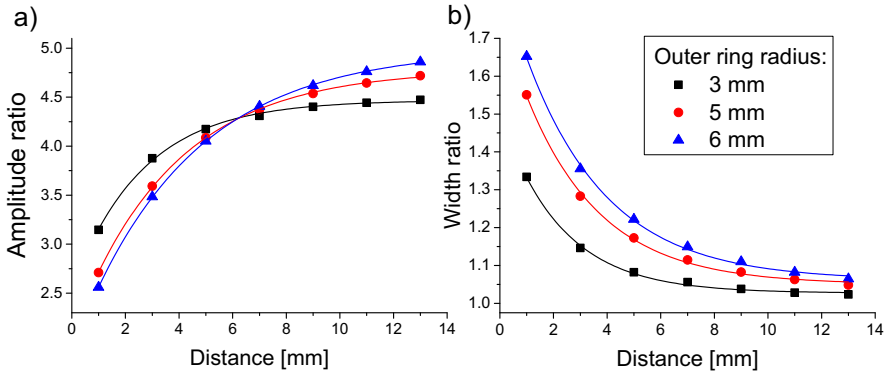

Fig. 1. (a) The signal amplitude ratio and (b) the signal width ratio as a function of the distance from the probe for outer rings of different sizes.

with air so that its tip had the same curvature as the pipe wall. As a charged object passed the probe, two current signals were induced to the sensors. To determine the induced charge, the signals were integrated over time. It was noticed that the shape of integrals were quite similar to Gaussian profile so Gaussian curves were fitted to the data to reduce noise. The amplitudes (A_o and A_i for outer and inner probe respectively) and widths (W_o and W_i) of the fitted curves were recorded. The amplitude ratio A_o/A_i and width ratio W_o/W_i were also calculated. Calibration equations were experimentally determined and used in measurements for these parameters as functions of charge, size, and distance of the passing object [15].

The obtained Gaussian width ratio data was suffered from high standard deviations and therefore could not be used for the calculations. The charged objects were required to pass the probe symmetrically, as otherwise the calculations yielded false results. As the lateral displacement from the probe axis increased, the signal amplitudes decreased, since more electric field lines coupled with the grounded metal pipe walls. However, relatively less electric field lines coupled with the inner sensor, thus increasing the amplitude ratio A_o/A_i. On the other hand, the width ratio W_o/W_i decreased.

The computer simulations in the present study were made using finite element software COMSOL Multiphysics 4.3b. Charged spheres with various sizes were set to pass the probe inside a metal pipe, with different distances from the probe. Tetrahedral mesh was used. The mesh size around the tip of the probe was set to "extremely fine" and around the sphere to "finer", as the software's built-in parameter sets were called. As a result, the element size was approximately 0.1 mm for the probe tip, and 2 mm for the sphere. The electric field **E** at the probe tip was calculated using equations

$$\nabla \cdot (\epsilon_0 \epsilon_r)\mathbf{E} = \rho \tag{1}$$

and

$$\mathbf{E} = -\nabla V, \tag{2}$$

where ρ is charge density, ϵ_0 is permittivity, ϵ_r is relative permittivity, and V is potential. The induced charge was calculated by first calculating the surface charge density σ from equation

$$\mathbf{E} = \frac{\sigma}{\epsilon_0 \epsilon_r}\hat{u}_n, \tag{3}$$

where $\hat{u}_n$ is the unit normal vector. The surface charge density σ was then integrated over the surface of the sensors. Relative permittivities were set to 10^4 for the probe and the metal pipe, 3.0 for the sphere, 2.1 for the insulators, and unity for air which filled the pipe. No special boundary conditions were applied to the insulator part of the probe.

Increasing the radius of the outer ring increased the ranges of ratios A_o/A_i and W_o/W_i. This is illustrated in Fig. 1(a) and (b), where three outer rings with different radii (3 mm, 5 mm and 6 mm) are compared. According to the simulation results, increasing the outer ring radius improves the probe sensitivity to changes in the size, distance and charge of the passing object, which enables more accurate calculations and a wider detection range. Asymmetrically passing objects could be taken into account by vertically splitting the outer ring into two adjacent parts. If the object has displacement to the right for instance, the signal amplitude ratio $A_o^R/A_o^L > 1$ since more field lines would couple with the outer right sensor. For a symmetrically passing object, $A_o^R/A_o^L = 1$.

2.2. Experimental methods

2.2.1. The experimental set-up

A new coaxial probe with a two-piece outer sensor was built based on the simulations from brass. The tip of the probe consisted of a disc-shaped inner sensor (radius 2 mm) which was surrounded by a 2 mm wide, vertically split outer sensor ring (outer radius 10 mm). The sensors were separated from each other by non-conducting epoxy. As illustrated in Fig. 2, the outer ring was split vertically into two adjacent parts and separated by a 1 mm wide insulator in the upper and lower parts of the ring. There was also an insulator around the outer probe. The probe was attached to a metal pipe with an inner diameter of 100 mm and height of 1.0 m, in order to use the probe later in measurements in a fluidized bed device. The curvature of the probe tip was matched with the curvature of the pipe wall.

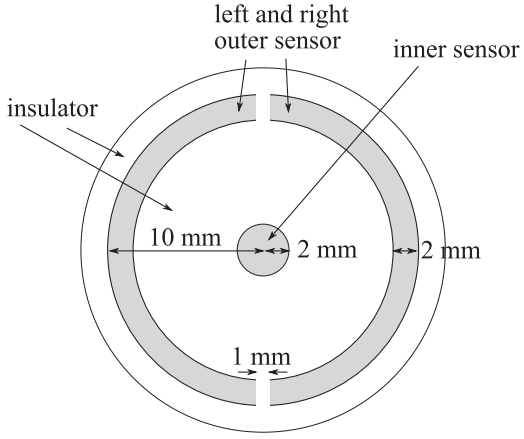

Fig. 2. The tip of the coaxial probe with a vertically split outer ring sensor.

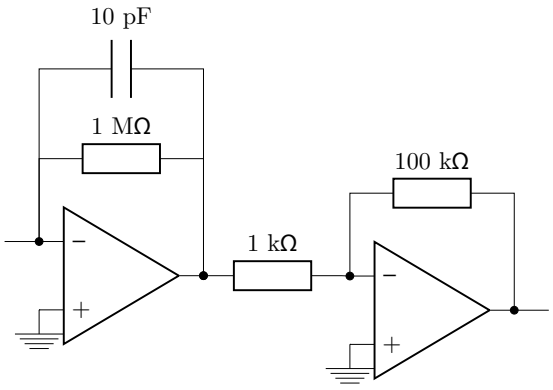

Fig. 3. The signal amplifier circuit.

Each of the three sensors was connected to a dedicated amplifier electrical circuit (Fig. 3). The amplifier circuits were powered by a 9 V battery. The signals were amplified in two stages. First, the signals were amplified by using a 1 MΩ resistor connected between the inverting input and the output of an operational amplifier. The signals were low-pass filtered by using a 10 pF capacitor. At the next stage, the signals were amplified with 100 kΩ and 1 kΩ resistors, for a total gain of 10^8. The circuit was placed inside a metal box. The induced current signals were converted into a digital form by using a NI USB-6008 (National Instruments) analog-to-digital converter at a sampling rate of 1 ms. The data was then analyzed using a virtual instrument (VI) compiled with LabVIEW 2009 (National Instruments).

2.2.2. Calibration

The calibration was done by dropping frictionally charged polypropylene spheres (Redhill Precision, Czech Republic) past the probe. Sphere radii (r) of 2.000 mm, 4.000 mm, 5.000 mm, 6.000 mm, 7.500 mm, 10.000 mm, 12.500 mm, 15.000 mm, and 17.500 mm (accuracy given by the manufacturer) were used. Spheres with different sizes and charges were dropped from different positions, at a height of 78 mm above the center of the probe. Here distance refers to the perpendicular distance between the probe and the edge of the sphere when the sphere was closest. The perpendicular passing distance from the probe (x) was varied from 4.0 mm to 40.0 mm, and lateral displacement (y) from the probe axis was varied from 0.0 mm to 20.0 mm, both in 4.0 mm steps. The set-up is illustrated in Fig. 4.

As a charged sphere passed the sensors, induced current signals were integrated over time and linear baseline corrections were made when necessary. In the next step, Gaussian curves

$$f(t) = A \cdot \exp\left(-\frac{(t-t_c)^2}{2W^2}\right) + f_0 \quad (4)$$

were fitted to the integrals using LabVIEW, and the Gaussian curve amplitudes (A_i for the inner, A_o^L and A_o^R for the outer left and right sensors respectively) and widths (W_i, W_o^L and W_o^R respectively) were recorded. Also, the amplitude A_o and width W_o for the sum signal of the outer sensors were collected. In Eq. (4), A is the amplitude, W is the width, t_c is the position of the center, and f_0 is the offset of the peak.

For the charge measurement, the spheres fell directly into a Faraday cup, which was connected to a Keithley 6517A electrometer (Keithley Instruments). In calibrations, charging the spheres uniformly was difficult. Also, the trajectory of the spheres most probably deviated slightly during measurements. Therefore, measurements were repeated approximately 50 times in order to reduce error limits.

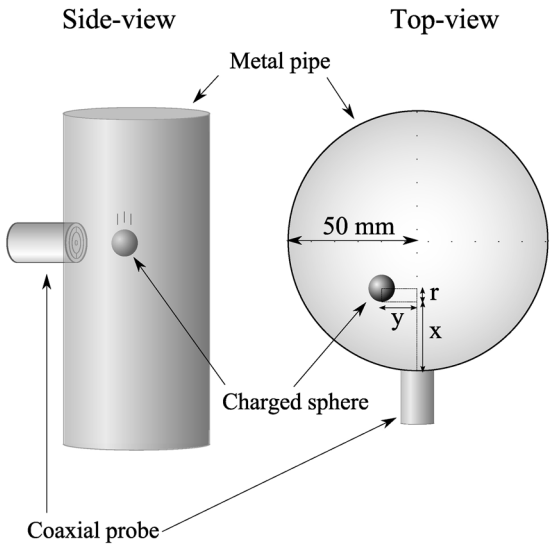

Fig. 4. The side-view (left figure) and the top-view (right figure) of the set-up.

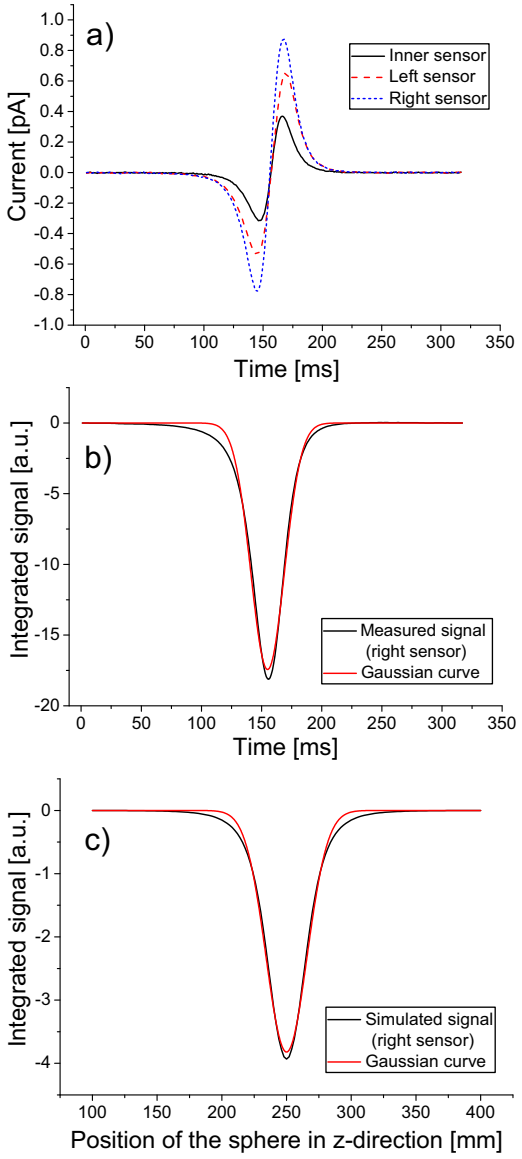

Fig. 5. (a) Examples of measured current signals, (b) integrated measured signal and Gaussian curve, and (c) simulated signal and Gaussian curve.

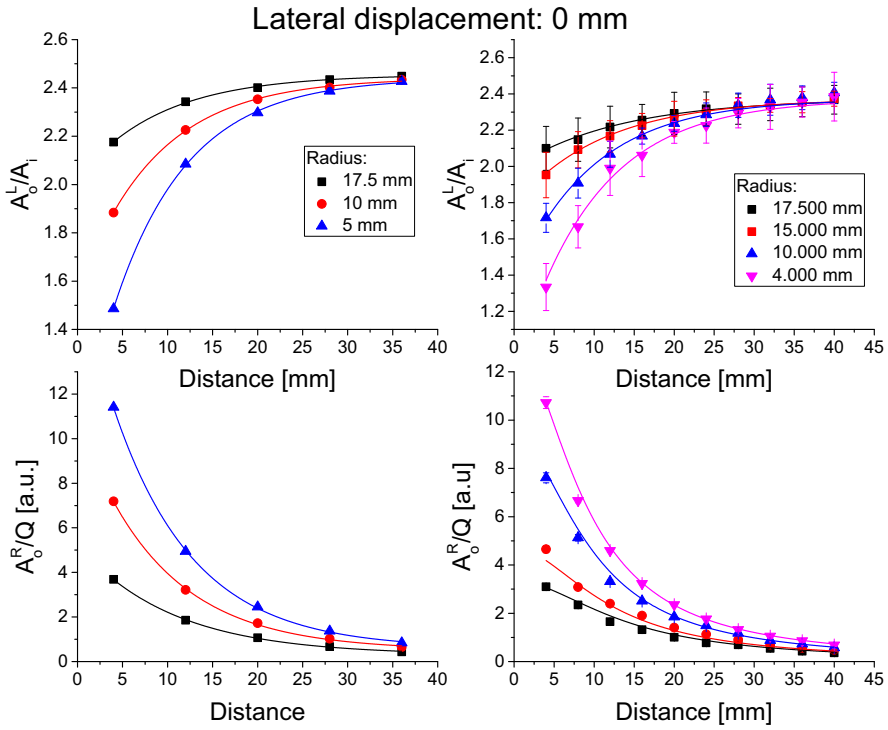

Fig. 6. Simulated (left) and experimental (right) A_o^L/A_i and A_o^R/Q as a function of distance and radius at displacement of 0 mm.

3. Results and discussion

3.1. Calibration

Example current signals and their integrals are compared to simulations in Fig. 5. As seen in Figs. 6 and 7, the simulated and experimentally measured data matched with each other. When the sphere trajectories were displaced from the probe axis, the amplitude ratio A_o^R/A_o^L decreased as the distance x increased and approached unity. This means that at larger distances the effect of the displacement became smaller. For a completely symmetrical passing, the ratio was exactly 1. In both simulations and

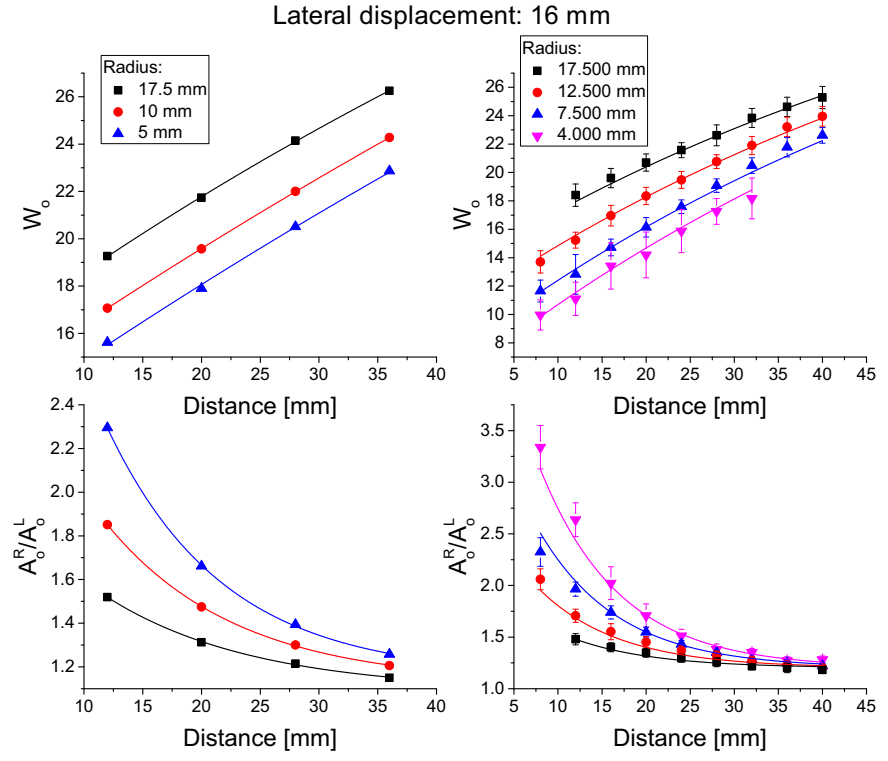

Fig. 7. Simulated (left) and experimental (right) W_o and A_o^R/A_o^L as a function of distance and radius at displacement of 16 mm.

experiments, the displacement was determined to increase from left to the right.

The amplitude ratio A_o^L/A_i increased with the sphere passing distance and the sphere radius. The ratio approached a value of approximately $A_o^L/A_i = 2.4$ with long distances. According to the simulations, the widths W_i, W_o^R and W_o^L depended linearly on the passing distance. However, experimental data showed slight deviation from this behavior at greater distances.

Only the amplitudes depended on the charge (Q), and the dependency was linear. The slopes A_i/Q, A_o^R/Q and A_o^L/Q decreased in an exponential-like manner as x was increased. They also decreased as r and y were increased.

The data from the calibration measurements was used to determine the calibration equations for $A_o^R/A_o^L(r, x, y)$, $A_o^L/A_i(r, x, y)$, $W_o(r, x, y)$ and $A_o^R(r, x, y, Q)$. The width ratio data was better than with the previously presented probe but also suffered from high standard deviation. For this reason, the width ratio was not used. Instead, W_o was used. Unfortunately, the widths were the only parameters which are affected by the speed of the object. Therefore, the speed of the object needed to be known. Inhomogeneous charging of the spheres and imperfections in determining the passing position are most likely the causes for somewhat significant error limits. The equations were completely experimental, and their form was not of great interest *per se*. Therefore, they are not presented here.

The used calibration limits were applicable ranges for the measurements with some restrictions. At distances larger than approximately 30 mm, the values of $A_o^R/A_o^L(r, x, y)$ and $A_o^L/A_i(r, x, y)$ didn't change much as radius was changed. Therefore, 30 mm can be considered as the upper limit of the distance. The smallest charge which was detected properly in the calibrations was 0.05 nC for sphere with radius of 2 mm.

3.2. Testing the calibration

After calibrations, a virtual instrument compiled with LabVIEW was programmed to solve the calibration equations. When simultaneous signals were detected with all the sensors, the amplitudes and widths of the integrated curves were collected as described earlier. Next, r, x and y were determined by simultaneously solving the equations for $A_o^R/A_o^L(r, x, y)$, $A_o^L/A_i(r, x, y)$ and $W_o(r, x, y)$. In the next step, the calculated r, x and y were used to calculate the charge from equation obtained for $A_o(r, x, y, Q)$. The calculated values were only accepted if they were within the calibration limits.

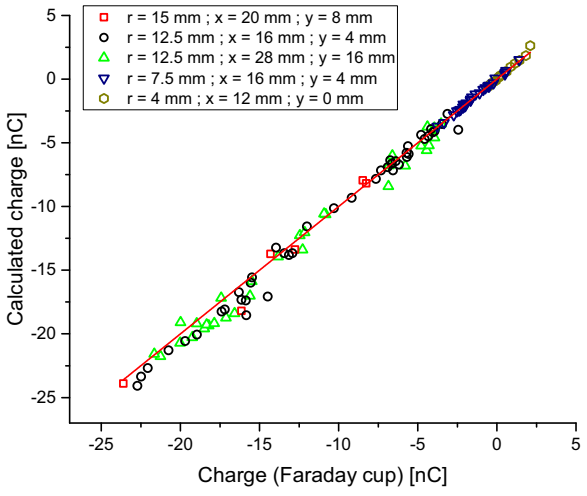

Fig. 8. Calculated charge as a function of the charge measured with the Faraday cup. The solid line represents the slope equal to 1, *i.e.* line where the values are equal.

Table 1
Examples of calculated radius, distance and displacement compared to real values. N refers to number of measurements.

	r (mm)	x (mm)	y (mm)	N
Real	17.5	12.0	4.0	28
Calc.	18.2 ± 2.0	10.3 ± 3.0	4.6 ± 1.0	
Real	15.0	20.0	8.0	6
Calc.	12.8 ± 3.0	21.0 ± 4.4	9.0 ± 2.4	
Real	12.5	28.0	16.0	33
Calc.	12.6 ± 2.5	27.4 ± 4.1	16.9 ± 2.0	
Real	7.5	24.0	8.0	27
Calc.	7.4 ± 3.2	22.6 ± 4.1	5.2 ± 1.2	
Real	4.0	12.0	0.0	15
Calc.	3.1 ± 2.5	12.2 ± 4.6	2.7 ± 0.9	

The calculated charge as a function of the measured charge is presented in Fig. 8. The slope is very close to 1 which means that the calculated charge values were close to the ones measured with the Faraday cup. Table 1 presents examples of calculated radii, distances and displacements and their correct values. As measurements were repeated, it was noticeable that although the standard deviation of the calculated values was sometimes quite large, they were on average close to the real values.

4. Conclusions

A coaxial probe with a vertically split outer sensor ring to measure the charge, size, distance and lateral displacement of a passing object with known speed was calibrated and tested. The results show that with the determined calibration equations, these properties can be calculated for spherical objects. Splitting the outer ring vertically made it possible to also measure the properties of asymmetrically passing objects, which is a major advantage as compared to the old probe design with a simple one-piece outer ring. Also, increasing the outer ring radius in relation to the inner sensor radius increased the detection range of both sphere radius and sphere distance.

The simulations were found to match with experimental measurements. This could possibly enable calibrating forthcoming probes which can be, for instance, too small to be calibrated reliably by the methods presented in this paper.

In future work, the probe will be used to measure the charge-to-mass ratio of fluidized powders in a bubbling fluidized bed.

Acknowledgments

Janne Peltonen is grateful to the University of Turku Graduate School (UTUGS-PCS) for financing the study. The authors would like to thank M.Sc. Outi Alanen (Laboratory of Industrial Physics, University of Turku) for her important help with forming the calibration equations. M.Sc. Jorma Roine (Laboratory of Industrial Physics, University of Turku) is acknowledged for his help in the writing process.

References

[1] D.A. Hays, J.C. Sheflin, Electrostatic adhesion of ion and triboelectric-charged particles, J. Electrostat. 63 (2005) 687–692, http://dx.doi.org/10.1016/j.elstat.2005.03.031.

[2] H. Kweon, S. Yiacoumi, C. Tsouris, The role of electrostatic charge in the adhesion of spherical particles onto planar surfaces in atmospheric systems, Colloids Surf. A: Physicochem. Eng. Asp. 481 (2015) 583–590, http://dx.doi.org/10.1016/j.colsurfa.2015.06.030.

[3] J. Paasi, Assessment of ESD threats to electronic components, J. Electrostat. 63 (2005) 589–596, http://dx.doi.org/10.1016/j.elstat.2005.03.021.
[4] H.-Y. Chen, P.-K. Li, Characteristic study on an ESD suppressor by the FDTD method, J. Electrostat. 71 (2013) 625–634, http://dx.doi.org/10.1016/j.elstat.2013.03.005.
[5] M. Nifuku, H. Tsujita, K. Fujino, K. Takaichi, C. Barre, M. Hatori, S. Fujiwara, S. Horiguchi, E. Paya, A study on the ignition characteristics for dust explosion of industrial wastes, J. Electrostat. 63 (2005) 455–462, http://dx.doi.org/10.1016/j.elstat.2005.03.002.
[6] J.B. Gajewski, Monitoring of electrostatic fire and explosion hazards at the inlet to electrostatic precipitators, J. Electrostat. 72 (2014) 192–197, http://dx.doi.org/10.1016/j.elstat.2014.02.003.
[7] J.A. Cross, Electrostatics: Principles, Problems and Applications, IOP Publishing Limited, Bristol, 1987.
[8] P. Secker, J. Chubb, Instrumentation for electrostatic measurements, J. Electrostat. 16 (1984) 1–19, http://dx.doi.org/10.1016/0304-3886(84)90015-9.
[9] M. Murtomaa, E. Laine, Electrostatic measurements on lactose–glucose mixtures, J. Electrostat. 48 (2) (2000) 155–162, http://dx.doi.org/10.1016/S0304-3886(99)00063-7.
[10] A. Giffin, P. Mehrani, Comparison of influence of fluidization time on electrostatic charge build-up in the bubbling vs. slugging flow regimes in gas–solid fluidized beds, J. Electrostat. 68 (2010) 492–502, http://dx.doi.org/10.1016/j.elstat.2010.06.013.
[11] J.D. Thomas, G.S. Hodges, D.G. Seely, N.a. Moroz, T.J. Kvale, Performance enhancement study of an electrostatic Faraday cup detector, Nucl. Instrum. Methods Phys. Res. A 536 (2005) 11–21, http://dx.doi.org/10.1016/j.nima.2004.07.211.
[12] S. Kausik, M. Chakraborty, P. Dutta, M. Kakati, B. Saikia, Study of charge distribution in a dust beam using a Faraday cup, Phys. Lett. A 372 (2008) 860–865, http://dx.doi.org/10.1016/j.physleta.2007.08.047.
[13] A. Kashefian Naieni, F. Bahrami, N. Yasrebi, B. Rashidian, Design and study of an enhanced Faraday cup detector, Vacuum 83 (2009) 1095–1099, http://dx.doi.org/10.1016/j.vacuum.2009.01.005.
[14] M. Murtomaa, J. Salonen, Simultaneous measurement of particle charge, distance and size using coaxial induction probe, J. Phys. Conf. Ser. 646 (2015) 012038, http://dx.doi.org/10.1088/1742-6596/646/1/012038.
[15] J. Peltonen, M. Murtomaa, J. Salonen, A coaxial induction probe for measuring the charge, size and distance of a passing object, J. Electrostat. 77 (2015) 94–100, http://dx.doi.org/10.1016/j.elstat.2015.07.009.
[16] M. Machida, B. Scarlett, Development of displacement current tomography system, Part. Part. Syst. Charact. 15 (1998) 36–41.

Biographies

Janne Peltonen M.Sc. received his M.Sc. from the University of Turku Finland in 2014. He is currently working as a Ph.D. student at the University of Turku. His current research interests include solid state physics, electrostatics and its applications and problems.

Matti Murtomaa Ph.D. received his Ph.D. from the University of Turku Finland in 2003. He studies and teaches electromagnetism and electrostatics at the Department of Physics and Astronomy at the University of Turku, Finland. He is also a member of the editorial board of Journal of Electrostatics. His interests include industrial electrostatics, charging of solids and electrostatic instrumentation.

Aleksi Saikkonen B.Sc. received his B.Sc. from the University of Turku in 2014. He is currently working towards his M.Sc. degree. His current research interests include biomedical imaging.

Jarno Salonen Ph.D. was born in 1967. He received his M.Sc. degree in 1995 and Ph.D. degree in 1999 from the University of Turku. He has studied porous silicon since 1994. His current research interests include porous silicon biomedical and sensor applications. He has published more than 180 scientific articles and he is also the head of the Industrial Physics Laboratory.